Beam cleanup of a 532-nm pulsed solid-state laser using a bimorph mirror

Xiang Lei (雷 翔)[1,2,3], Bing Xu (许 冰)[1,2*], Ping Yang (杨 平)[1,2], Lizhi Dong (董理治)[1,2], Wenjin Liu (刘文劲)[1,2,3], and Hu Yan (晏 虎)[1,2,3]

[1]*Laboratory on Adaptive Optics, Institute of Optics and Electronics, Chinese Academy of Sciences, Chengdu 610209, China*

[2]*Key Laboratory on Adaptive Optics, Chinese Academy of Sciences, Chengdu 610209, China*

[3]*Graduate University of Chinese Academy of Sciences, Beijing 100049, China*

[*]*Corresponding author: bing-xu-ioe@yahoo.cn*

Received May 25, 2011; accepted June 22, 2011; posted online August 30, 2011

A successful beam cleanup of a 5-mJ/200-μs pulsed solid-state laser system operating at 532-nm wavelength is demonstrated. In this beam cleanup system, a wave-front sensor-less adaptive optics (AO) system is set up with a 20-element bimorph mirror (BM), a high-voltage amplifier, a charge-coupled device camera, and a control software implementing the stochastic parallel gradient descent (SPGD) algorithm. The brightness of the laser focal spot is improved because the wave-front distortions have been compensated. The performance of this system is presented and the experimental results are analyzed.

OCIS codes: 140.3460, 010.1080, 140.3538.

doi: 10.3788/COL201210.021401.

High beam quality is well known to be one of the most important objects to pursue in applications of pulsed solid-state lasers. However, many wave-front distortions generated from the lasers make it difficult to realize this goal. There are several sources of wave-front distortions in a pulsed solid-state laser; for instance, the nonlinear effects of materials and thermal lensing[1] contribute to the degradation of beam quality. Scientists have developed many ways to achieve high beam quality. Chiou *et al.* used photorefractive two-wave mixing for cleaning up wave-front aberrations of laser beams[2,3]. Steinhausser *et al.* obtained high energy pulses with good beam quality through a stimulated Brillouin scattering injection-seeded beam cleanup process[4]. Adaptive optics (AO) technique, originally developed in astronomy[5,6], is now being used for pulsed laser beam cleanup and has been proved to be an effective method[7−14].

A typical AO system includes three main parts: a wave-front sensor (WFS), an active correction element, and a control strategy. When these AO systems are applied to correct wave-front aberrations, the aberrations are measured by the WFSs directly. Then, based on the wave-front information, wave-front aberration correction can be done. Shack-Hartmann sensors and lateral shearing interferometers have been used as WFSs in traditional beam cleanup systems for pulsed laser system. However, in a strong scintillation regime or when the intensity of the laser beam is rather nonuniform, conventional AO systems based on the WFSs above cannot obtain obvious results[15,16]. Moreover, the strategy of correct information driving deformable mirrors (DMs) from wave-front measurement is in general a difficult task, requiring a sophisticated control architecture that might be too complex for applications which demand compactness and a special design for each laser system. Due to the reasons above, optimization-based AO systems without any WFS have been developed for application in many laser systems to improve output beam quality[17−19]. In this letter, an optimization-based AO system for beam cleanup of a 532-nm pulse operation green solid-state laser with a repetition rate of 100 Hz is presented. Without any WFS, this AO system is based on a stochastic parallel gradient descent (SPGD) algorithm, a far-field charge-coupled device (CCD) camera, and a 20-element bimorph mirror (BM). The schematic experimental system and control strategy is described in detail.

As one of the most popular correctors used in AO systems, BMs[20−23] have some advantages for laser beam correction and formation (e.g., better correction capability for low-order aberrations and low cost). A 20-element BM fabricated in our laboratory is adopted in this beam cleanup system as the corrector. Figure 1(a) shows the image and structure of this BM[20,21].

As shown in Fig. 1(b), this BM mainly consists of two layers of piezoelectric transition (PZT) and a thin glass sheet. The flat glass sheet is firmly glued to one layer of PZT with high-reflection coating. The two layers of PZT have the same structure and dimension and are made from the same material. The locations of control layers with the metal electrodes soldered to the PZT surfaces are indicated as e1 and e2. A whole defocus electrode e2 is used for large defocus correction. The remaining 19 discrete electrodes on e1 are bonded to the bottom PZT layer with their distribution shown in Fig. 1(c). The common electrode situated in the center of the two layers of PZT is grounded. The initial root mean square deviation from the surface plane is 0.44 μm with no voltages applied on the actuators, which can be corrected by itself. The distortions induced by the surface structure will decrease as the technology develops[21].

This side-pumped Nd:YAG laser operates with multiple transverse modes. It works at a repetition rate of 100 Hz with a wavelength of 532 nm. The width of each

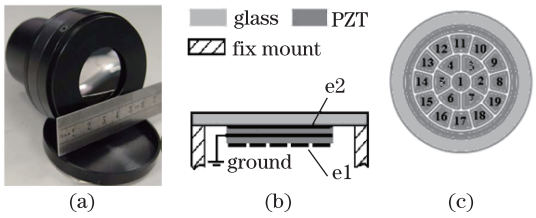

Fig. 1. BM used in the beam cleanup system. (a) BM image; (b) profile of the BM, e1 and e2 indicate the locations of control layers; (c) control electrode distribution on e1.

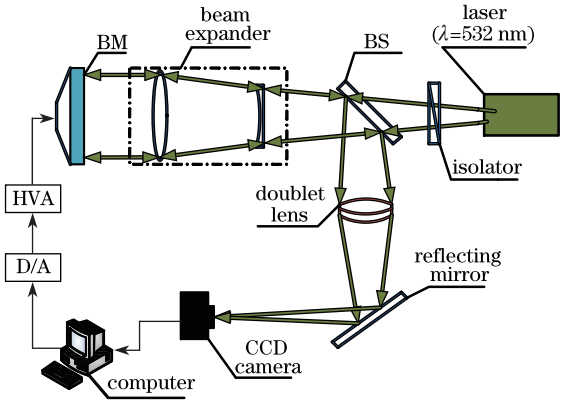

Fig. 2. Schematic of the beam cleanup system. The laser beam is represented by green lines, and the direction of propagation is indicated by an arrow.

laser pulse is 200 μs.

Figure 2 presents a schematic of the experimental beam cleanup system. The beam path in the experiment is almost the same as that in practice[24]. Although not the best, this beam path design shown in Fig. 2 could make the structure more compact in our laboratory. The pulsed laser beam first passes through an isolator, which could prevent the laser beam from being reflected back and damaging the laser. Then, the laser beam passes a beam splitter (BS). The BS has two functions: to attenuate the intensity of the laser to make it fit for measurement and to reflect the incident light from the BM. To control the aberrations brought by the optical elements in the ray path, the beam expander is well chosen. The aberration brought by the beam expander is very small (<0.5 μm). Since the beam diameter of 6 mm, the beam expander with an amplification factor of 4 is used to collimate the laser and expand the beam diameter to 24 mm. By expanding the beam diameter, the BM's spatial correction capability can be exploited completely. As the key element of this beam cleanup system, the BM (diameter, 30 mm) has a large deflection range. Each actuator can be individually controlled by a voltage within –500 and 500 V, and the defocus range is no less than 10 μm. The incident beam is vertical to the BM surface. After being reflected by the BM, the incident beam is then reflected by the BS before it is focused by a doublet lens. The aperture of the doublet lens is 25 mm with a focal length of 300 mm. A CCD camera with a resolution of 64 × 64 pixels receives the focal spot of the laser beam. The images indicate the intensity distribution of the light spot acquired by an image grabber card, with its acquisition rate controllable by an industrial computer. The computer updates the digital voltages to optimize the intensity signal. First, these voltages are converted into analog voltage signals by 16-bit analogue output (D/A) cards in the industrial computer and then amplified by a high-voltage amplifier (HVA) before being applied to the BM. The optimization algorithm adopted in this system is SPGD.

SPGD algorithm is a global search algorithm that is independent of the system model. A measured quality metric J is a function of the control parameters $\{u = u_1, u_2, \cdots, u_N\}$, typically the control voltages applied to BM electrodes. The method is based on the rather simple and elegant idea described below.

First, a series of statistically independent random voltages[19] $\{\delta u_i^n\}$ $(i = 1, \cdots, 20)$ as the small positive perturbations is simultaneously (in parallel) added to the control voltages $\{u_i^n\}$, $(i = 1, \cdots, 20)$. The voltage signals become $\{u_i^n + \delta u_i^n\}$ $(i = 1, \cdots, 20)$, which are converted by D/A cards and amplified by the HVA before being applied to the BM. The surface deformation of the BM would change the focal spot. We acquire the focal spot intensity from the CCD camera to calculate the encircled energy as the positive one (J_+^n).

Then, the same series of small voltages $\{\delta u_i^n\}$ is used as the negative perturbations acting on the same control voltages $\{u_i^n\}$ $(i = 1, \cdots, 20)$ as follows $\{u_i^n - \delta u_i^n\}$ $(i = 1, \cdots, 20)$, which are also applied on the BM. The focal spot intensity is captured by the CCD camera again and used to calculate the encircled energy as the negative one (J_-^n). After recording both J_+^n and J_-^n, the nth iteration is ended.

Finally, the control voltages are updated as $u_i^{n+1} = u_i^n + \gamma \delta u_i^n (J_+^n - J_-^n)$, where $i = 1, \cdots, 20$ and γ is a gain coefficient. These iteration steps would optimize the surface of the BM and maximize the performance metric (the encircled energy) in our system. When the encircled energy reaches maximization, the BM is considered to have compensated for the distortions successfully.

In the point-source AO systems based on SPGD algorithm, the Strehl ratio (SR), quadratic sum of intensity, mean radius, and encircled energy are usually used as the system performance index[19]. However, the SR is difficult to achieve in a real experimental system. Practitioners usually use the other three indexes, whereas in this beam cleanup system, the encircled energy of the focal spot on the CCD camera is used as the feedback signal to control the BM and can be described as

$$J = \int_R I(x, y) \mathrm{d}x\mathrm{d}y, \tag{1}$$

where R is the square region, with its center being the centroid of the focal spot on the CCD camera. The position of the centroid $(x_\mathrm{c}, y_\mathrm{c})$ is defined as

$$x_\mathrm{c} = \frac{\int x I(x, y) \mathrm{d}x\mathrm{d}y}{\int I(x, y) \mathrm{d}x\mathrm{d}y}, \tag{2}$$

$$y_\mathrm{c} = \frac{\int y I(x, y) \mathrm{d}x\mathrm{d}y}{\int I(x, y) \mathrm{d}x\mathrm{d}y}, \tag{3}$$

where $I(x, y)$ is the intensity distribution received by the CCD camera.

The repetition rate of the pulsed laser is set to 100 Hz.

To grab each pulse, the exposure time of the CCD camera is adjusted to match the acquisition rate. However, the acquisition process is still slightly asynchronous. Hence, the control method is optimized accordingly. If the performance metric is found to be invalid in the SPGD algorithm, the performance metric and the BM voltages would be suspended until the next valid renovation. The modifications to the control system are critical for the optimization-based pulsed laser beam cleanup system. The far-field light spot, shown in Fig. 3(a), occupies nearly one-third of the effective area on the CCD camera before correction. With the SPGD process proceeding, the far-field light spot converges and the performance metric is enhanced simultaneously. Finally, the far-field light spot converges to a stable bright one, as shown in Fig. 3(b).

Figure 4 compares the intensities of images before and after correction in the horizontal and vertical directions. Figure 4(a) shows the lineout of focal spots in a horizontal direction, and Fig. 4(b) shows the lineout of focal spots in a vertical direction. The peak value of gray level before correction is about 143 (0–255), which is represented by a blue curve. After correction, the peak value of gray level, represented by a red curve, achieves 254. The peak value of gray level improves by 77.6%. In addition, the light spot is convergent and its peak value increases distinctively, as shown in Fig. 5. Figures 5(a) and (b) are captured by a laser beam profiler, and these two images are in the same scale. The M^2 factor

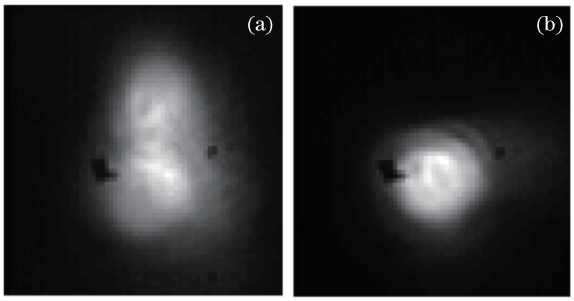

Fig. 3. Focal spot captured by the CCD camera when the repetition rate of the laser is 100 Hz (a) before correction and (b) after correction.

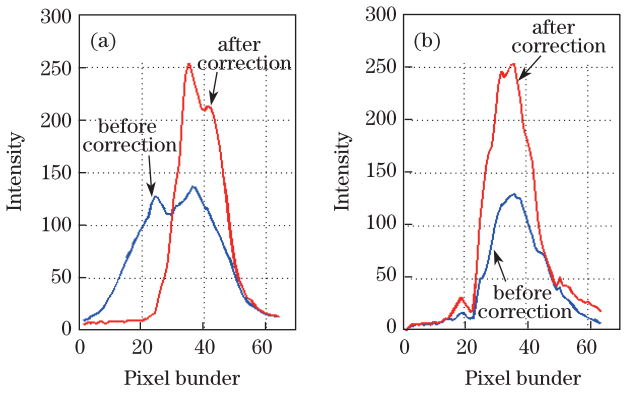

Fig. 4. Comparison of the profile of focal spot in Fig. 3. (a) Horizontal lineout of focal spots; (b) vertical lineout of focal spots.

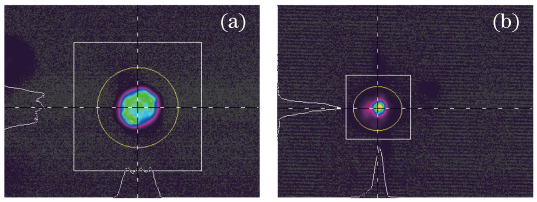

Fig. 5. Shape of the focal spot captured by another camera; (a) before correction and (b) after correction.

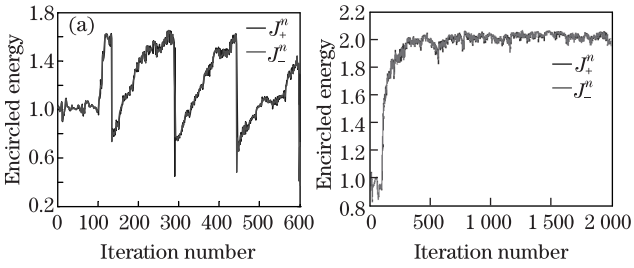

Fig. 6. Convergence curve at 100-Hz pulse repetition rate (with the encircled energy normalization). (a) Before an optimization in SPGD algorithm; (b) with an optimization in the SPGD algorithm.

measured by the laser beam profiler is 32 before correction, decreasing to less than 8 when the beam cleanup has been accomplished.

Figure 6 demonstrates that the numerical value of encircled energy increases with the iteration number. Figure 6(a) shows that the performance metric drops periodically before the SPGD algorithm is optimized. The images of the focal spot captured between pulses induce invalid performance metric calculations. In contrast, Fig. 6(b) shows that the control method has been optimized, and the performance metric (encircled energy) fluctuates a little and then becomes much larger than before correction. After about 300 iterations, the numerical value of encircled energy becomes stable. Finally, the encircled energy within a 9-pixel by 9-pixel area has a 120% improvement after correction by the BM.

In conclusion, a successful beam cleanup of a 5-mJ/200-μs pulsed solid-state laser system operating at 532 nm using a WFS-less AO system is demonstrated. In the control process, the modified SPGD is selected to optimize the far-field light spot and the encircled energy is taken as the performance metric. The pulse repetition rate is set to 100 Hz. After correction, the performance metric is increased more than 100% and the convergence curve becomes stable. This indicates that most distortions of the laser beam have been corrected by the proposed beam cleanup system.

This work was supported by the National Natural Science Foundation of China (Nos. 60978049 and 10974202), the Innovation Science Fund of Chinese Academy of Sciences (No. CXJJ-10-S01), and the Western Light Talent Cultivation Program of Chinese Academy of Sciences (No. A09k005). Part of the research was supported by the Open Research Fund of Key Laboratory of Functional Crystals and Laser Technology, TIPC, CAS.

References

1. W. Koechener, *Solid-State Laser Engineering* (Springer, Berlin, 2005) chap. 4.
2. A. E. T. Chiou and P. Yeh, Opt. Lett. **10,** 621 (1985).
3. A. E. Chiou and P. Yeh, Opt. Lett. **11,** 461 (1986).
4. B. Steinhausser, A. Brignon, E. Lallier, J. P. Huignard, and P. Georges, Opt. Express **15,** 6464 (2007).
5. C. Rao, L. Zhu, X. Rao, C. Guan, D. Chen, J. Lin, and Z. Liu, Chin. Opt. Lett. **8,** 966 (2010).
6. K. Wei, X. Zhang, H. Xian, W. Ma, A. Zhang, L. Zhou, C. Guan, M. Li, D. Chen, S. Chen, Z. Liao, C. Rao, and Y. Zhang, Chin. Opt. Lett. **8,** 1019 (2010).
7. K. Akaoka, S. Harayama, K. Tei, Y. Maruyama, and T. Arisawa, Proc. SPIE **3265,** 219 (1998).
8. F. Druon, G. Chériaux, J. Faure, J. Nees, M. Nantel, A. Maksimchuk, G. Mourou, J. C. Chanteloup, and G. Vdovin, Opt. Lett. **23,** 1043 (1998).
9. H. Baumhacker, G. Prezler, K. J. Witte, M. Hegelich, M. Kaluza, S. Karsch, A. Kudryashov, V. Samarkin, and A. Roukossouev, Opt. Lett. **27,** 1570 (2002).
10. S. Ito, H. Ishikawa, T. Miura, K. Takasago, A. Endo, and K. Torizuka, Appl. Phys. B **76,** 497 (2003).
11. A. G. Aleksandrov, V. E. Zavalova, A. V. Kudryashov, A. L. Rukosuev, P. N. Romanov, and V. V. Samarkin, J. Opt. Technol. **71,** 737 (2004).
12. B. Wattellier, J. Fuchs, J. P. Zou, K. Abdeli, C. Haefner, and H. Pépin, Rev. Scient. Instrum. **75,** 5186 (2004).
13. T. A. Planchon, J. -P. Rousseau, F. Burgy, G. Chériaux, and J.-P. Chambaret, Opt. Commun. **252,** 222 (2005).
14. A. Alexandrov, S. Fourmaux, J. C. Kieffer, A. Kudryashov, F. Martin, T. Ozaki, and S. Payeur, in *Proceedings of CAOL* 213 (2010).
15. J. Sheldakova, A. Kudryashov, V. Samarkin, and V. Zavalova, Proc. SPIE **6872,** 68720B (2008).
16. C. A. Primmerman, T. R. Price, R. A. Humphreys, B. G. Zollars, H. T. Barclay, and J. Herrmann, Appl. Opt. **34,** 2081 (1995).
17. M. A. Vorontsov and V. P. Sivokon, J. Opt. Soc. Am. A **15,** 2745 (1998).
18. G. W. Carhart, G. J. Simer, and M. A. Vorontsov, Proc. SPIE **5162,** 28 (2003).
19. P. Piatrou and M. Roggemann, Appl. Opt. **46,** 6831 (2007).
20. Y. Ning, W. Jiang, N. Ling, and C. Rao, Opt. Express **15,** 12030 (2007).
21. Y. Ning, "Performance test and application study of a bimorph deformable mirror", PhD. Thesis (National University of Defense Technology, 2008).
22. V. Samarkin, A. Aleksandrov, and A. Kudryashov, Proc. SPIE **4493,** 269 (2002).
23. J. C. Dainty, A. V. Koryabin, and A. V. Kudryashov, Appl. Opt. **37,** 4663 (1998).
24. P. Yang, Y. Ning, X. Lei, B. Xu, X. Li, L. Dong, H. Yan, W. Liu, W. Jiang, L. Liu, C. Wang, X. Liang, and X. Tang, Opt. Express **18,** 7121 (2010).